Journal of the Meteorological Society of Japan

EARLY ONLINE RELEASE

The DOI for this manuscript is
DOI:10.2151/jmsj.2025-030
J-STAGE Advance published date: June 12, 2025
The final manuscript after publication will replace the preliminary version at the above DOI once it is available.

Relationship of the Interannual Variation in Quasi-Stationary Heavy Precipitation Systems over Kyushu, Southwestern Japan with the Sea Level Pressure Pattern

Kazuya WAKAO[1]

[1]Graduate School of Environmental Science
Hokkaido University, Sapporo, Japan

Kenta TAMURA[2,3] and Tomonori SATO[2]

[2]Faculty of Environmental Earth Science
Hokkaido University, Sapporo, Japan
[3]Current affiliation: Snow and Ice Research Center, National Research Institute for Earth Science and Disaster Resilience, Nagaoka, Japan

Submitted to Journal of the Meteorological Society of Japan
Submitted on June 26, 2024
Revised on December 11, 2024, April 12, 2025, and May 31, 2025

Corresponding author: Kazuya Wakao
Graduate School of Environmental Science, Hokkaido University
Kita-10, Nishi-5, Kita-ku, Sapporo 060-0810 JAPAN
Email: wakao_kazuya@ees.hokudai.ac.jp
Tel: +81-11-716-2111

Abstract

This study classified atmospheric fields to investigate the distribution of, and the interannual variation in, heavy rainfall that occur over Kyushu, southwestern Japan, which have shown marked increase in recent years. Radar/rain gauge-analyzed precipitation data acquired during June–September (2006–2023) were used to identify quasi-stationary heavy precipitation systems (QSPSs), and the 6-hourly sea level pressure (SLP) pattern was classified to elucidate the impact of synoptic conditions on the interannual variation in the frequency of QSPSs. It was found that the occurrence location of QSPSs corresponded to the inflow side of lower-level water vapor transport. Specifically, under the SLP pattern representing a cyclonic circulation to the south of Kyushu, QSPSs occurred over the eastern mountain region in Kyushu Island. Conversely, QSPSs occurred over western Kyushu when the SLP pattern reflected the extension of the North Pacific high to the south of Japan. The interannual variation in the occurrence number of QSPSs was interpreted based on the frequency of the above mentioned favorable SLP patterns. The interannual variation in the occurrence number of QSPSs corresponded with changes in the appearance frequency of the favorable SLP patterns as evidenced by many QSPSs occurrences in 2020 under a prevailing North Pacific high, suggesting a possible, albeit not strong, influence of the synoptic circulation on QSPSs. Furthermore, this variation is strongly affected by dynamical and thermodynamical factors specific to each SLP pattern, which play a critical role in determining the probability of the QSPSs occurrence.

Keywords heavy precipitation; mesoscale convective systems; synoptic patterns; water vapor transport; interannual variation

1. Introduction

Global warming and associated changes in heavy precipitation are alarming issues worldwide, which poses significant risks to society through various environmental threats, including natural disasters, food insecurity, and disruptions to ecosystem services (e.g., Seneviratne et al. 2021; Bezner et al. 2022). Observational studies have documented the changes in frequency and intensity of heavy rainfall across various regions and climate zones (e.g., Zhang et al. 2013; Li et al. 2018; Sun et al. 2021), and this trend is projected to intensify in the future. Therefore, it is crucial to reduce uncertainty in future projection of heavy precipitation by improving our understanding of its variability.

In Japan, given that the region is affected by the East Asian summer monsoon and mid-latitude weather systems, heavy rainfall events frequently occur in association with anomalous water vapor transport maintained by various synoptic fields. For example, strong water vapor transport toward Japan is observed around the western periphery of the North Pacific high (Zhao et al. 2021), and tropical cyclones can convey remarkable amounts of water vapor toward the country, even when the cyclone is located far from mainland Japan (Hatsuzuka et al. 2020). To understand the contributions of moisture transport driven by different systems to heavy rainfall over Japan, classification of atmospheric fields is an effective approach. Previous studies revealed that the rate of future increase in heavy rainfall is projected to be different for each rainfall-causing disturbance (e.g., Miyasaka et al. 2020; Hatsuzuka and Sato 2022). Specifically, Kawase et al. (2019) emphasized that the influence of global warming is different between heavy rainfall events caused by tropical cyclones and those associated with Baiu front, even within the same region. It is also anticipated that heavy rainfall events, previously unprecedented, may be increasingly frequent due to atmospheric rivers in the future climate (Kamae et al. 2021). These studies imply that the rates of heavy rainfall change are affected by the occurrence frequency of the rainfall-causing synoptic systems. Therefore, it is suggested that long-term variations in the frequency of heavy rainfall should be investigated with consideration of the variations in atmospheric fields that lead to heavy rainfall events. Since local heavy precipitation is largely influenced by the broader-scale environment, which is a characteristic common across much of the globe (Laing and Fritsch 2000; Markowski and Richardson 2010; Trier et al. 2014), separating the drivers of precipitation variability into those associated with synoptic patterns and other conditions can add significant value to understanding precipitation variability.

The record heavy rainfall occurred in western Kyushu, western Japan, in July 2020. During this event, heavy precipitation caused destructive floods in the Kuma River region, southwestern Kyushu (Araki et al. 2021). At the time of the event, the underlying characteristic synoptic condition promoted substantial transport of low-level water vapor toward western Kyushu around the periphery of the North Pacific high (JMA 2020). These circumstances denote the crucial role of the synoptic conditions that regulate water vapor transport on the genesis and development of convective systems. Therefore, understanding the relations among the synoptic field, water vapor transport, and occurrence of heavy precipitation are essential for elucidating the potential long-term changes in heavy precipitation that might be expected in the era of climate change.

The number of heavy rainfall events over Kyushu has increased in recent years (Fujibe 2015), which is related to the variability of low-level water vapor flux (Kato 2024), leading to the increasing risk of associated landslides and flood disasters. Extreme precipitation with significant accumulation is often associated with quasi-stationary mesoscale precipitation systems (Yoshizaki et al. 2000; Hirota et al. 2016; Kato 2020). It is crucial to examine how these systems have been altered in relation to climate change. Therefore, the interannual variation in quasi-stationary precipitation systems (QSPSs) over Kyushu should be elucidated through better understanding of their formation and development mechanisms. Given that heavy rainfall over Kyushu occurs under various atmospheric fields (e.g., the Baiu front, which is formed in association with East Asian summer monsoon, and typhoons), investigating the characteristics of QSPSs under each background atmospheric field might provide new insights into the impact of climate change to heavy precipitation. Thus, by classifying the atmospheric fields, the objective of this study was to investigate the geographical distribution of, and the interannual variation in, QSPSs that occur over Kyushu.

2. Data and methods

2.1 Identification of QSPSs

This study adopted the method for identification of QSPSs proposed by Hirockawa et al. (2020a). This method identifies heavy rainfall considering their stationarity as described in brief below. The dataset employed is radar/rain gauge-analyzed precipitation data (Nagata 2011) provided by the Japan Meteorological Agency (JMA). Following Hirockawa and Kato (2022), the original radar/rain gauge-analyzed precipitation data with 1-km (0.0125° × 0.00833°) resolution were converted to 5-km (0.0625° × 0.05°) resolution, and 3-hourly accumulated precipitation data were used in the analysis. The requirements for QSPSs include an area of strong rainfall (at least 80 mm 3-h^{-1}) greater than 500 km^2, with at least one grid point with precipitation exceeding 100 mm 3-h^{-1}. These requirements have been widely used in studies on extreme rainfall events in this region (Hirockawa et al. 2020b; Kawase et al. 2023; Watanabe et al. 2024), and we confirmed they are applicable for recent heavy rainfall events that occurred over the mountainous area on 5 July 2017, which brought severe floods and landslides in northern Kyushu (Takemi 2018). Please note that this study does not take into account either the aspect ratio or the least duration of the precipitation systems, both of which were considered in Hirockawa et al. (2020a). The first time/date that satisfies these requirements is regarded as the time of QSPSs genesis. Figure 1a illustrates the domain used for analysis of QSPSs. In this study, we analyze QSPSs that exist over the land and the sea within 30 km offshore of the coastline, taking into account the limited accuracy of the radar/rain gauge-analyzed precipitation over the sea. In analyzing the warm season (April–November) in 2006–2023, we identified 1,394 QSPSs (Fig. 1b).

The geographical distribution of the frequency of QSPSs genesis (Fig. 1b) shows that the genesis frequency is high over western Kyushu and the mountain region of eastern Kyushu, consistent with Hirockawa et al. (2020a). Numerous QSPSs genesis events are observed over the ocean when we extend the area (Fig. S1), highlighting the need for detailed investigations using data with sufficient accuracy over the ocean in the future. The monthly variation shows that approximately 90% of the QSPSs occurred during June–September with a peak in July (Fig. 1c). It was also found that the lifespan was $\leq$ 5 h for approximately 95% of the QSPSs (Fig. 1d).

2.2 Synoptic pattern classification

To investigate the relationship between QSPS genesis and synoptic conditions, we conducted classification of atmospheric fields. This section describes the classification method. In this study, sea surface pressure (SLP) was adopted as the variable subjected to the classification because SLP controls the lower-tropospheric atmospheric circulation that drives the transport of low-level water vapor, which is crucial for the formation of rainbands (e.g., Johns and Doswell 1992; Schumacher and Rasmussen 2020). In addition, it has been reported that moisture transport near the surface (below 850-hPa) is considered to play a crucial role in heavy rainfall in Kyushu region (Kato 2018), which might be because the region is surrounded by warm oceans. The SLP data at approximately 0.375° horizontal resolution and 6-h intervals were acquired from the Japanese Reanalysis for Three Quarters of a Century (JRA-3Q: Kosaka et al. 2024) provided by the JMA. We used the self-organizing maps (SOMs) approach (Kohonen 1982) to classify the spatial pattern of SLP. The SOMs methodology is implemented as an artificial neural network, which is intended to transform high-dimensional datasets into visually understandable low-dimensional (e.g., two-dimensional) maps. The SOMs approach has been used widely for classification of atmospheric fields (e.g., Cavazos 2000), including identification of atmospheric fields related to heavy rainfall in Japan (e.g., Ohba et al. 2015). As an input vector in the SOMs method, spatially standardized SLP fields at 6-h intervals over the study domain (22°–42°N, 120°–140°E; see Fig. 2) that is substantially larger than Kyushu Island, were used for the SOMs training. The classification was conducted for the period of June–September with consideration of the frequency of QSPSs (Fig. 1c) in 2006–2023. Eventually, 2 × 4 SLP patterns (8 nodes) were created for 8,784 input vectors (4 times per day ×

122 summer days × 18 years).

The SOMs further facilitate the classification of 6-hourly SLP patterns, as summarized in Fig. 2, which depicts a composite of classified SLP patterns. Patterns #1 and #2 are characterized by low pressure located from south of the Nansei Islands to near Taiwan which is far from Kyusyu region. Patterns #5 and #6 are characterized by low pressure located relatively close to Kyushu region, extending from Kyushu to its southeastern sea, whereas patterns #3, #4, #7, and #8 are characterized by the existence of the North Pacific high. On the basis of the above, we refer to patterns #1 and #2 as the Far Low (FL)-pattern, patterns #5 and #6 as the Near Low (NL)-pattern, and patterns #3, #4, #7, and #8 as the North Pacific high (NPH)-pattern. Notably, the SLP snapshots classified into the FL- and the NL-patterns are likely related to tropical cyclones because approximately 30% of the snapshots (i.e., 1,384 out of 4,332) involved tropical cyclones within the domain (22°–42°N, 120°–140°E) based the best-track dataset produced by the JMA. Additionally, we confirmed that these SLP patterns (i.e., the FL- and the NL-patterns) frequently appear in August and September (Figs. 3a and 3b) when many tropical cyclones approach Kyushu. Therefore, the areas of low pressure depicted in the FL- and the NL-patterns are considered to reflect tropical cyclones. The proportion of snapshots having a tropical cyclone center within the domain is low (approximately 15% in each) in the NPH-pattern; these SLP patterns frequently appear in June and July (Fig. 3c) corresponding to the Baiu season.

2.3 Decomposition of interannual variation in number of occurrences of QSPSs

To link the interannual variations in QSPSs with synoptic conditions, we attempted to decompose the interannual variations in QSPSs based on the result of the SLP classification. This subsection describes the methodology adopted in this study (Fig. 4).

In the first step, the interannual time series of QSPS occurrences was separated into three independent time series, each of which corresponds to the interannual counts of QSPSs occurring under each classified SLP pattern (i.e., the FL-pattern, the NL-pattern, and the NPH-pattern). Thus, total interannual variation in the occurrence number of QSPSs, $N(t)$, where t represents years, is determined as follows:

$$N(t) = \sum_{pattern=1}^{3} N_{pattern}(t)$$

$$= N_{FL}(t) + N_{NL}(t) + N_{NPH}(t), \quad (1)$$

where $N_{FL}(t)$, $N_{NL}(t)$, and $N_{NPH}(t)$ indicate the interannual variations in the occurrence number of QSPSs under the FL-pattern, the NL-pattern, and the NPH-pattern, respectively. Considering that SLP is available at 6-hour interval in JRA-3Q, we used the SLP snapshot at the closest time with QSPS genesis. In this study, the expression of 'occurrence' is used for QSPSs to denote their genesis at the time of this snapshot. The results of aforementioned decomposition are presented in Subsection 3.2.

In the second step, we decomposed the interannual variations in the occurrence number of QSPSs in each SLP pattern into three factors:

$$N_{pattern}(t) = A_{pattern}(t) \times P_{pattern}(t) \times S_{pattern}(t), \quad (2)$$

where $A_{pattern}(t)$ indicates the number of appearances of each SLP pattern regardless of the presence or absence of QSPSs. This term represents the counts of snapshots in each year for each typical SLP pattern. Hence, it is supposed to represent the characteristics of the synoptic condition in each summer. The second term, $P_{pattern}(t)$, indicates the probability of occurrence of at least one QSPS under each SLP pattern. This term is calculated as the rate of the number of the SLP snapshots coinciding with QSPS to SLP snapshot classified into each SLP pattern ($A_{pattern}$). The third term, $S_{pattern}(t)$, indicates the annual average of simultaneous QSPS occurrences under each SLP pattern. The terms $P_{pattern}(t) \times S_{pattern}(t)$ reflect the mean number of QSPS occurrences per given SLP pattern. Through this decomposition, we examine the attribution of synoptic weather conditions and other factors to total interannual variation in QSPSs, and the results are presented in Section 4.

3. Results

3.1 Distribution of QSPSs in each SLP pattern

Figure 5a shows a composite of the water vapor flux (FLWV) under each SLP pattern when QSPSs occurred. The calculation of FLWV follows Kato (2018, 2020), which is described as below.

$$FLWV = \rho q v,$$

where ρ, q, and v represent dry air density, mixing ratio of water vapor, and wind speed, respectively, obtained from JRA-3Q. If the terrain height is less than 300-m, the FLWV was computed at a height of 500-m. Otherwise, it is calculated at the terrain heights plus 200-m (Kato 2018). For simplicity, these heights are, hereafter, referred to as 500-m heights. It is evident that the water vapor transport is consistent with the atmospheric flow associated with the SLP distribution when QSPSs occurred (Fig. S2). The water vapor transport in the FL-pattern (#1 and #2) is characterized by a southeasterly flow toward Kyushu induced by low pressure far to the south of Kyushu. Meanwhile, southerly water vapor transport is driven by low pressure located near western Japan in the NL-pattern (#5 and #6). The NPH-pattern (#3, #4, #7, and #8) is characterized by southerly or southwesterly water vapor transport from the East China Sea, around the periphery of the North Pacific high.

To better compare water vapor transport with SLP patterns, a composite of vertically integrated water vapor transport is drawn using snapshots taken only during the occurrence of QSPSs (Fig. 5b). The FL-pattern and the NL-pattern are characterized by a southerly and southeasterly water vapor flow, respectively. Meanwhile, southwesterly water vapor transports are dominant toward Kyushu in the NPH-pattern, which denotes the mid-tropospheric moisture transport due to East Asian summer monsoon and lower-tropospheric moisture transport surrounding North Pacific high (Kato et al. 2003).

The spatial distributions of QSPSs are examined for each SLP pattern, as shown in Fig. 6. In the FL-pattern and the NL-pattern, the QSPS occurrences are observed more often over the mountainous region of eastern Kyushu because of orographic lifting of the moist southeasterly flow. In the NPH-pattern, most of QSPSs over western Kyushu appear attributable to the water vapor flux strengthen in the East China Sea. This pattern often causes heavy rainfall events over western Kyushu (Kawase et al. 2019), and it is associated with mesoscale convective systems during the Baiu season (Tsuguchi and Kato 2014). Interestingly, Fig. 6 suggests that the location of the QSPSs might be identifiable based solely on the SLP pattern and associated moisture transport pathways, which underscores the effectiveness of the synoptic-scale pattern classification for the prediction of extreme weather events caused by QSPSs.

3.2 Interannual variation in the number of QSPS occurrences

Based on the identified SLP patterns and QSPSs, interannual variation in the number of QSPSs during June–September is investigated. On average, QSPSs occurred at the rate of 58.6 counts year^{-1} in the first half of the study period (2006–2014), but this increased to 80.8 counts year^{-1} in the second half (2015–2023) (Fig. 7a). The linear trend for this increase is significant ($p_{MK} < 0.05$) with a rate of 15.0 counts decade^{-1} according to the nonparametric Theil-Sen's estimator (Theil 1950; Sen 1968) and Mann-Kendall trend test (Mann 1945). Additionally, the accumulated precipitation due to QSPSs shows a positive trend (Fig. 7b), which is not statistically significant. It should be noted that these results might be affected by low-frequency internal variability contributing to the trend in this short analysis period.

The interannual variation in the occurrence number of QSPSs differs among three SLP patterns (Fig. 7c). The amplitudes of interannual variation are relatively large in the FL-pattern (#1 and #2) and the NL-pattern (#5 and #6). This could be influenced by the number of tropical cyclones passing around Kyushu in these two patterns. We noticed that an increasing trend was observed in the occurrence number of QSPSs in the NL-pattern when ocean area was included (not shown; see Fig. S1 for the domain). Although this trend is not discussed in detail due to the insufficient accuracy of radar/rain-gauge-analyzed precipitation data over the sea, the result implies possible changes in QSPS occurrences over the sea, perhaps related to the ocean warming. In contrast, approximately 50 QSPSs per year on average occur in the NPH-pattern (#3, #4, #7, and #8), accounting for approximately 70% of all QSPSs. This high frequency agrees with the fact that heavy rainfall in Kyushu frequently occurs around the Baiu front

(Tsuguti and Kato 2014), which is common in the NPH-pattern. During the Baiu season, the number of short duration heavy rainfall events has increased in recent years in Kyushu region (Fujibe et al. 2005; Kato 2024). In the present study, however, the occurrence number of QSPSs does not show an increasing trend in the NPH-pattern, which is dominant during the Baiu season (Fig. 3c). The analysis using long period data may detect the increasing trend of the occurrence number of QSPSs in the NPH-pattern. These characteristics suggest that QSPSs occurring in the NPH-pattern might make a substantial contribution to the variability in the overall number of QSPSs.

4. **Discussion**

4.1 Interannual variations and role of tropical cyclones

Through a decomposition of the observed interannual variation of the QSPSs, it is found that the appearance of the synoptic pattern (A(t)) is not a crucial factor leading to QSPS occurrences (Figs. 8a–c). However, the high appearance frequency of the NPH-pattern (A_{NPH}) in 2020 (335 snapshots or 83.75 days during June–September) coincides well with the frequent occurrences of QSPSs (87 counts). Therefore, the frequency of the NPH-pattern during summer 2020 might be an underlying factor behind the highest occurrence of QSPSs, implying that the role of synoptic conditions should be validated over a longer period. The interannual variations in the occurrence probability and the simultaneous occurrence number (i.e., P(t) and S(t), respectively) are relatively large or significantly correlated with that in the number of QSPS occurrences, which is a common characteristic (Figs. 8d–i), except for $S_{FL}(t)$, which shows a relatively high correlation coefficient that is not statistically significant (Fig. 8g).

Notably, the probability term for the NL-pattern ($P_{NL}(t)$) exhibits a positive trend (Fig. 8e) during 2006–2023. Figure 9a shows the frequency of tropical cyclones when QSPSs occurred in the NL-pattern, defined as the fractional duration of the presence of tropical cyclone centers. It denotes that the NL-pattern involves QSPS events associated with a tropical cyclone existing over and near the Kyushu region. Interestingly, the interannual variation of $P_{NL}(t)$ is relatively large correlated (r=0.54) with the fractional duration of tropical cyclones that are present over the Kyushu region or the East China Sea (Fig. 9b). $P_{NL}(t)$ suggests that the low pressure features in the regions reflect the probability whether a tropical cyclone exists. In other words, the likelihood of QSPS occurrences in the Kyushu region in the NL-pattern increases if a tropical cyclone exists near the

Kyushu region. Furthermore, the positive trend in $P_{NL}(t)$ denotes the increasing contribution of tropical cyclones to QSPS occurrences in the Kyushu region (Fig. 9b). This is consistent with the IPCC report (Seneviratne et al. 2021) which mentioned, based on climate model simulations, that tropical-cyclone-induced rainfall is projected to increase with enhanced greenhouse gas concentrations. The contributions of sea surface temperature warming in the surrounding oceans and elevated atmospheric moisture content in each of these SLP patterns should be investigated in future studies.

4.2 The role of environmental conditions

For each SLP pattern, we investigate whether there are differences in the environmental conditions in the QSPS occurrences. Here, six indices that are proposed to be representative of the environmental conditions leading to QSPS geneses (Kato 2020) were analyzed using JRA-3Q. The indices and their threshold include (1) the water vapor flux at 500-m heights (FLWV; > 150 g m^{-2} s^{-1}), (2) the storm-relative environmental helicity (SREH; > 100 m^2 s^{-2}), (3) the distance between 500-m heights and the level for free convection for airmass lifted from 500-m heights (dLFC; < 1,000 m), (4) the equilibrium level for the airmass lifted from 500-m heights (EL; > 3,000 m), (5) the relative humidity at 500 hPa and 700 hPa (RH; > 60 %), and (6) the upward velocity at 700 hPa averaged horizontally by about 400 km (W700; > 0 m s^{-1}).

Figure 10 summarizes the importance of each index, calculated as the fractional duration that satisfies the requirements relative to the total duration for each pressure pattern. The results are presented as the difference between the fractional durations with and without QSPS occurrences. In the FL-pattern, there are large differences in RH and W700 over Kyushu, suggesting their essential role in forming QSPSs. In the NL-pattern, differences are prominent in FLWV, SREH, RH, and W700. These differences are relatively large compared to the other SLP patterns and the other indices. This is speculated to be because QSPS occurrences in the NL-pattern are highly dependent on tropical cyclones (Fig. 9a), which brings large-scale and intense impacts on the multiple environmental indices. In the NPH-pattern, zonally extending patterns are found in FLWV, RH, and W700. This is presumably corresponding to the presence of a stagnant front extending zonally since nearly half of the fractional duration of the NPH-pattern coincides with the Baiu season (Fig. 3c). Through this analysis, we have identified differences in the environmental conditions, associated with QSPS occurrences in each SLP-pattern. As a common character across all SLP patterns, the differences in SREH are relatively local but with remarkable magnitude over the land area in the Kyushu region. It suggests the importance of vertical wind shear which may have contributed to the organization of mesoscale convective systems. The further analysis was conducted for indices of FLWV, SREH, RH, and W700, which are found influential to QSPS occurrences.

Here, we explore the relationship between environmental conditions and P(t). The four indices (FLWV, SREH, W700, and RH) were averaged over Kyushu or surrounding regions, taking into consideration the characteristics of each index. For SREH, W700 and RH, the averaging domains are set over Kyushu Island. Meanwhile, the domain for FLWV is positioned upstream of the heavy rainfall, encompassing southeastern Kyushu for the FL- and the NL-patterns and southwestern Kyushu for the NPH-pattern. This setting reflects the direction of the dominant moisture transport associated with each SLP pattern (Fig. 5a). To compare their interannual variations with P(t), the fractional duration during which each index exceeded the threshold is calculated (Fig. 11). Please note that this analysis focuses on two months when QSPSs occurred most frequently in each SLP pattern, namely July and September for the FL-pattern, August and

September for the NL-pattern, and June and July for the NPH-pattern, respectively. In the FL-pattern, correlations against P(t) are statistically significant for W700 (r=0.55) and RH (r=0.76). The likelihood of QSPS occurrences in the FL-pattern may be attributable to the large-scale upward motion related to fronts around the Kyushu region which is maintained by the northwestward water vapor transport (#1 and #2 in Fig. 5a). In the NL-pattern, a statistically significant correlation was not found for any of the indices. This suggests that the interannual variation of $P_{NL}(t)$ is more strongly influenced by the presence of tropical cyclones near Kyushu (see Subsection 4.1) than these indices. In the NPH-pattern, higher correlations were confirmed for FLWV (r=0.60), RH (r=0.60), and SREH (r=0.62). This suggests that the essential factors for QSPS occurrences in the NPH-pattern are the moisture supply, the preconditioning of mid-level moist air, and the organization of convective systems due to vertical wind shear. The above analysis showed that the environmental conditions that contribute to the probability of QSPS occurrences are different depending on the SLP patterns.

5. Summary

In this study, by applying classification of synoptic atmospheric fields, we examined the interannual variation in the occurrence number of QSPSs that trigger local destructive disasters in Kyushu, southwestern Japan. The QSPSs, identified from radar/rain gauge-analyzed precipitation data, showed a statistically significant increase trend during June–September 2006–2023. To elucidate the contribution of the background synoptic conditions, we classified 6-hourly SLP maps using the SOMs classification technique into three SLP patterns, and validated the relationship between the likelihood of each SLP pattern and QSPS occurrence frequency in each year. It was found that the occurrence regions of QSPSs are likely determined by the SLP pattern because the pathways of the lower-tropospheric moisture transport that causes heavy rainfall are regulated by the SLP pattern. Specifically, the FL-pattern and the NL-pattern tend to cause QSPSs over eastern Kyushu related to southeasterly and southerly winds surrounding the areas of low pressure centered far to the south of Kyushu and near western Japan, respectively. Meanwhile the NPH-pattern tends to cause QSPSs over western Kyushu related to the southwesterly winds prevailing around the periphery of the North Pacific high. These results indicate that QSPSs are likely to form on the upwind side of mountain regions in relation to the direction of moisture transport. Among these SLP patterns, QSPSs occurring in the NPH-pattern account for approximately 70% of the total, thereby contributing substantially to the variability in the overall number of QSPSs.

On the basis of the identified QSPSs and the SLP classification, we examined the interannual variation in the number of QSPSs, by considering the year-to-year difference in 6-hourly appearance frequency in each SLP pattern (A(t)). It was found that A(t) is not correlated with the interannual variation in the occurrence number of QSPSs in all SLP patterns. It is worth noting that in 2020 A(t) for the NPH-pattern coincided with the number of QSPSs. Thus, synoptic patterns may contribute to the variability in QSPS occurrences under certain unclarified conditions, including the effects of low-frequency variability modes, such as Pacific decadal oscillation and El Niño southern oscillation on heavy precipitation. This would also contribute to a better understanding of precipitation variability in East Asia (Fujibe 2015; Sun et al. 2019), which includes regions with flat plain, unlike the mountainous areas analyzed in the current study. Further investigation using a long-term data analysis is required to understand these contributions more clearly.

In contrast, the interannual variations in the probability of QSPS occurrences and the simultaneous occurrence number in each SLP pattern (P(t) and S(t)) were correlated with that in the occurrence number of QSPSs of most SLP patterns. Specifically, P(t) was found to have the highest correlation with the occurrence number of QSPSs in all SLP patterns. To obtain a better physical understanding of P(t), the relationship between P(t) and environmental conditions was examined. The results indicate that P(t) reflects the influence of large-scale upward motion and humidity in the FL-pattern, the fractional duration of tropical cyclones around Kyushu in the NL-pattern, and low-level water vapor flux, humidity, and vertical wind shear in the NPH-pattern. These results suggest essential environmental conditions leading to QSPS occurrences in each SLP pattern. In the FL-pattern and the NL-pattern, water vapor transport driven by cyclonic circulation in the south of Kyushu flowing toward the frontal zone around Kyushu and the presence of tropical cyclone around Kyushu are important, respectively. Meanwhile, in the NPH-pattern, strong moisture transport around the western periphery of the North Pacific high and the presence of strong vertical wind shear are important for QSPS occurrences.

This study proposed a new methodology to quantify the contribution of synoptic SLP patterns to the occurrence of QSPSs. The methodology can be applied to other regions or even to other types of extreme weather events that are formed in various synoptic patterns. While previous studies have focused on evaluating the interannual variation of tropical cyclone-induced heavy precipitation (e.g., Chang et al. 2012; Wang et al. 2024), the novelty of our study lies in its achievement of providing a framework that enables the quantitative comparison of multiple sources of heavy precipitation. Although systematically identifying heavy rainfall-bearing disturbances and their interannual variations remains a challenge, the recent studies have suggested that the SLP pattern is a key to identifying these systems. For example, characteristic low-level moisture transport has been observed in association with North Atlantic subtropical high in North America (Chiappa et al. 2024) and the slow propagation of a low pressure system in Europe (Mohr et al. 2023). In subsequent studies, the classification method can be extended to other meteorological variables deemed suitable for representing the targeted weather phenomena. Notably, mesoscale convective systems often initiate under similar environmental conditions, including baroclinicity, rather than being solely influenced by SLP patterns (Laing and Fritsch 2000; Blamey and Reason 2012). This highlights the importance of incorporating upper-air synoptic fields into pattern classification in future studies. It is hoped that the proposed methodology will advance the understanding of variability in extreme weather and contribute to reducing the uncertainties in future projection of such events. Further research applying the analysis methodology proposed in this study would improve the overall understanding of the interannual variation in the frequency of heavy precipitation triggered by mesoscale meteorological processes under the influence of climate change.

Data Availability Statement

The datasets used for this study were obtained from the Japanese Reanalysis for Three Quarters of a Century (JRA-3Q) project, carried out by the Japan Meteorological Agency (JMA). The JRA-3Q data were downloaded from the portal site of the Center for Computational Sciences (CCS), University of Tsukuba. The best-track datasets is available from the Regional Specialized Meteorological Center (RSMC) Tokyo, https://www.jma.go.jp/jma/jma-eng/jma-center/rsmc-hp-pub-eg/besttrack.html, and the radar/rain gauge-analyzed rainfall (JMA 2018) is available to the public from the JMA and was obtained from the Japan Meteorological Business Support Center (JMBSC), http://www.jmbsc.or.jp/en/index-e.html. We compiled the figures in Matplotlib version 3.7.2 (Hunter 2007; Caswell et al. 2023), available under the Matplotlib license at https://matplotlib.org/. We used the python “somoclu” package for the SOM analysis (Wittek et al. 2017).

Supplement

Supplement Figure 1 shows the distribution of the occurrence number of QSPSs detected within the analysis domain, which includes East China Sea.

Supplement Figure 2 shows the composite of SLP when QSPSs occurred in each SLP pattern.

Acknowledgments

We are grateful to the editor, Dr. Teruyuki Kato, and the two anonymous reviewers for their constructive comments and suggestions, which helped improve the manuscript. This study was supported by the Japan Society for the Promotion of Science KAKENHI (Grant Number: JP19H05697, JP24H02228), the Sentan program (Grant Number: JPMXD0722680734), and the Arctic Challenge for Sustainability II (ArCSII) project (Grant Number:

JPMXD1420318865). We thank James Buxton MSc, from Edanz (https://jp.edanz.com/ac), for editing a draft of this manuscript.

Reference

Araki, K., T. Kato, Y. Hirockawa, and W. Mashiko, 2021: Characteristics of atmospheric environments of quasi-stationary convective bands in Kyushu, Japan during the July 2020 heavy rainfall event. *SOLA*, **17**, 8–15.

Bezner Kerr, R., T. Hasegawa, R. Lasco, I. Bhatt, D. Deryng, A. Farrell, H. Gurney-Smith, H. Ju, S. Lluch-Cota, F. Meza, G. Nelson, H. Neufeldt, and P. Thornton, 2022: Food, Fibre, and Other Ecosystem Products. In: Climate Change 2022: Impacts, Adaptation and Vulnerability. Contribution of Working Group II to the Sixth Assessment Report of the Intergovernmental Panel on Climate Change [H.-O. Pörtner, D.C. Roberts, M. Tignor, E.S. Poloczanska, K. Mintenbeck, A. Alegría, M. Craig, S. Langsdorf, S. Löschke, V. Möller, A. Okem, B. Rama (eds.)]. Cambridge University Press, Cambridge, UK and New York, NY, USA, pp. 713–906, doi:10.1017/9781009325844.007.

Blamey, R. C., and C. J. C. Reason, 2012: Mesoscale Convective Complexes over Southern Africa. *J. Climate*, **25**(2), 753–766.

Caswell, T. A., and Coauthors, 2023: matplotlib/matplotlib: REL: v3.7.2 (zenodo.org), https://matplotlib.org/.

Cavazos, T., 2000: Using self-organizing maps to investigate extreme climate events: An application to wintertime precipitation in the Balkans. *J. Climate,* **13**(10), 1718–1732.

Chang, C.-P., Y. Lei, C.-H. Sui, X. Lin, and F. Ren, 2012: Tropical cyclone and extreme rainfall trends in East Asian summer monsoon since mid-20th century. *Geophys. Res. Lett.*, **39**, L18702.

Chiappa, J., D. B. Parsons, J. C. Furtado, and A. Shapiro, 2024: Short-duration extreme rainfall events in the central and eastern United States during the summer: 2003–2023 trends and variability. *Geophys. Res. Lett.*, **51**, e2024GL110424.

Fujibe, F., N. Yamazaki, M. Katsuyama, and K. Kobayashi, 2005: The increasing trend of intense precipitation in Japan based on four-hourly data for a hundred years. *SOLA*, **1**, 41–44.

Fujibe, F., 2015: Relationship between interannual variations of extreme hourly precipitation and air/sea-surface temperature in Japan. *SOLA,* **11**, 5–9.

Hatsuzuka, D., T. Sato, K. Yoshida, M. Ishii, and R. Mizuta, 2020: Regional projection of tropical-cyclone-induced extreme precipitation around Japan based on large ensemble simulations. *SOLA*, **16**, 23–29.

Hatsuzuka, D., and T. Sato, 2022: Impact of SST on present and future extreme precipitation in Hokkaido investigated considering weather patterns. *J. Geophys. Res. Atmos.,* **127**. e2021JD036120, doi:10.1029/2021jd036120.

Hirockawa, Y., T. Kato, H. Tsuguti, and N. Seino, 2020a: Identification and classification of heavy rainfall areas and their characteristic features in Japan. *J. Meteor. Soc. Japan,* **98**(4), 835–857.

Hirockawa, Y., T. Kato, K. Araki, and W. Mashiko, 2020b: Characteristics of an extreme rainfall event in Kyushu district, southwestern Japan in early July 2020. *SOLA*, **16**, 265–270.

Hirockawa, Y., and T. Kato, 2022: A new application method of radar/raingauge analyzed precipitation amounts for long-term statistical analyses of localized heavy rainfall areas. *SOLA*, **18**, 13−18.

Hirota, N., Y. N. Takayabu, M. Kato, and S. Arakane, 2016: Roles of an atmospheric river and a cutoff low in the extreme precipitation event in Hiroshima on 19 August 2014. *Mon. Wea. Rev.,* **144**(3), 1145–1160.

Hunter, 2007: Matplotlib: A 2D Graphics Environment. *Comput. Sci. Eng.*, **9**(3), 90–95, https://doi.org/10.1109/MCSE.2007.55.

Japan Meteorological Agency, 2018: Radar/raingauge-analyzed precipitation [Dataset]. Japan Meteorological Agency, https://www.jma.go.jp/jma/en/Activities/qmws_2018/Presentation/3.1/Radar%20Rain%20Gauge-Analyzed%20Precipitation_revised.pdf

Japan Meteorological Agency, 2020: Characteristics of the heavy rain of July 2020 and related atmospheric circulation (in Japanese). Press Release on 31 July 2020 of JMA, Retrieved from www.jma.go.jp/jma/press/2007/31a/r02gou.pdf.

Johns, R. H., and C. A. Doswell III, 1992: Severe local storms forecasting. *Wea. Forecasting*, **7**(4), 588–612.

Kamae, Y., Y. Imada, H. Kawase, and W. Mei, 2021**:** Atmospheric rivers bring more frequent and intense extreme rainfall events over East Asia under global warming. *Geophys. Res. Lett.,* **48**(24), e2021GL096030.

Kato, T., M. Yoshizaki, K. Bessho, T. Inoue, Y. Sato, and X-BAIU-01 observation group, 2003: Reason for the failure of the simulation of heavy rainfall during X-BAIU-01 —Importance of a vertical profile of water vapor for numerical simulations—. *J. Meteor. Soc. Japan*, **81**(5), 993–1013.

Kato, T., 2018: Representative height of the low-level water vapor field for examining the initiation of moist convection leading to heavy rainfall in East Asia. *J. Meteor. Soc. Japan*, **96**(2), 69−83.

Kato, T., 2020: Quasi-stationary band-shaped precipitation systems, named "senjo-kousuitai", causing localized heavy rainfall in Japan. *J. Meteor. Soc. Japan*, **98**(3), 485–509.

Kato, T., 2024: Interannual and diurnal variations in the frequency of heavy rainfall events in the Kyushu area, western Japan during the rainy season. *SOLA*, **20**, 191–197.

Kawase, H., Y. Imada, H. Sasaki, T. Nakaegawa, A. Murata, M. Nosaka, and I. Takayabu, 2019: Contribution of historical global warming to local-scale heavy precipitation in western Japan estimated by large ensemble high-resolution simulations. *J. Geophys. Res. Atmos.,* **124**(12), 6093–6103.

Kawase, H., M. Nosaka, S. I. Watanabe, K. Yamamoto, T. Shimura, Y. Naka, Y.-H. Wu, H. Okachi, T. Hoshino, R. Ito, S. Sugimoto, C. Suzuki, S. Fukui, T. Takemi, Y. Ishikawa, N. Mori, E. Nakakita, T. J. Yamada, A. Murata, T. Nakaegawa, and I. Takayabu, 2023: Identifying robust changes of extreme precipitation in Japan from large ensemble 5 km-grid regional experiments for 4K warming scenario. *J. Geophys. Res. Atmos.*, **128**(18), e2023JD038513.

Kohonen, T., 1982: Self-organized formation of topologically correct feature maps. *Biological Cybernetics,* **43**(1), 59–69.

Kosaka, Y., S. Kobayashi, Y. Harada, C. Kobayashi, H. Naoe, K. Yoshimoto, M. Harada, N. Goto, J. Chiba, K. Miyaoka, R. Sekiguchi, M. Deushi, H. Kamahori, T. Nakaegawa, T. Y. Tanaka, T. Tokuhiro, Y. Sato, Y. Matsushita, and K. Onogi, 2024: The JRA-3Q reanalysis. *J. Meteor. Soc. Japan*, **102**(1), 49–109.

Laing, A. G., and J. M. Fritsch, 2000: The large scale environments of the global populations of mesoscale convective complexes. *Mon. Weather Rev.* **128**(8), 2756–2776.

Li, W., Z. Jiang, X. Zhang, and L. Li, 2018: On the emergence of anthropogenic signal in extreme precipitation change over China. *Geophys. Res. Lett.*, **45**(17), 9179–9185.

Mann, H. B., 1945: Nonparametric tests against trend. *Econometrica*, **13**(3), 245–259.

Markowski, P., and Y. Richardson, 2010: *Mesoscale Meteorology in Midlatitudes*. Wiley-Blackwell, 407 pp.

Miyasaka, T., H. Kawase, T. Nakaegawa, Y. Imada, and I. Takayabu, 2020: Future projections of heavy precipitation in Kanto and associated weather patterns using large ensemble high-resolution simulations. *SOLA,* **16**, 125–131.

Mohr, S., U. Ehret, M. Kunz, P. Ludwig, A. Caldas-Alvarez, J. E. Daniell, F. Ehmele, H. Feldmann, M. J. Franca, C. Gattke, M. Hundhausen, P. Knippertz, K. Küpfer, B. Mühr, J. G. Pinto, J. Quinting, A. M. Schäfer, M. Scheibel, F. Seidel, and C. Wisotzky, 2023: A multi-disciplinary analysis of the exceptional flood event of July 2021 in central Europe – Part 1: Event description and analysis, *Nat. Hazards Earth Syst. Sci.*, **23**(2), 525–551.

Nagata, K., 2011: Quantitative precipitation estimation and quantitative precipitation forecasting by the Japan Meteorological Agency. Technical Review of RSMC Tokyo, 13 (Available online at: https://www.jma.go.jp/jma/jma-eng/jma-center/rsmc-hp-pub-eg/techrev/text13-2.pdf, accessed 31 May 2025).

Ohba, M., S. Kadokura, Y. Yoshida, D. Nohara, and Y. Toyoda, 2015: Anomalous weather patterns in relation to heavy precipitation events in Japan during the Baiu season. *J. Hydrometeor.,* **16**(2), 688–701.

Schumacher, R. S., and K. L. Rasmussen, 2020: The formation, character and changing nature of mesoscale convective systems. *Nat. Rev. Earth Environ.,* **1**(6), 300–314.

Sen, P. K., 1968: Estimates of the regression coefficient based on Kendall's Tau. *J. Amer. Statist. Assoc.*, **63**(324), 1379–1389.

Seneviratne, S.I., X. Zhang, M. Adnan, W. Badi, C. Dereczynski, A. Di Luca, S. Ghosh, I. Iskandar, J. Kossin, S. Lewis, F. Otto, I. Pinto, M. Satoh, S.M.

Vicente-Serrano, M. Wehner, and B. Zhou, 2021: Weather and Climate Extreme Events in a Changing Climate. In Climate Change 2021: The Physical Science Basis. Contribution of Working Group I to the Sixth Assessment Report of the Intergovernmental Panel on Climate Change [Masson-Delmotte, V., P. Zhai, A. Pirani, S.L. Connors, C. Péan, S. Berger, N. Caud, Y. Chen, L. Goldfarb, M.I. Gomis, M. Huang, K. Leitzell, E. Lonnoy, J.B.R. Matthews, T.K. Maycock, T. Waterfield, O. Yelekçi, R. Yu, and B. Zhou (eds.)]. Cambridge University Press, Cambridge, United Kingdom and New York, NY, USA, pp. 1513–1766, doi:10.1017/9781009157896.013.

Sun, B., H. Wang, B. Zhou, and H. Li, 2019: Interdecadal variation in the synoptic features of Mei-Yu in the Yangtze river valley region and relationship with the Pacific decadal oscillation. *J. Climate*, **32**(19), 6251–6270.

Sun, Q., X. Zhang, F. Zwiers, S. Westra, and L. Alexander, 2021: A Global, continental, and regional analysis of changes in extreme precipitation. *J. Climate*, **34**(1), 243–258.

Takemi, T., 2018: Importance of terrain representation in simulating a stationary convective system for the July 2017 northern Kyushu heavy rainfall case. *SOLA*, **14**, 153–158.

Theil, H., 1950: A rank-invariant method of linear and polynomial regression analysis, Part I., *Proc. Ned. Akad. Wet.*, **53**, 386–392.

Trier, S. B., C. A. Davis, D. A. Ahijevych, and K. W. Manning, 2014: Use of the parcel buoyancy minimum (B_{min}) to diagnose simulated thermodynamic destabilization. Part II: Composite analysis of mature MCS environments. *Mon. Weather Rev.* **142**(3), 967–990.

Tsuguti, H., and T. Kato, 2014: Objective extraction of heavy rainfall events and statistical analysis on their characteristic features. *Tenki,* **61**(6), 455–469 (in Japanese).

Wang, S., X. Chen, H. Yao, W. Ruan, Z. Gu, X. Li, Y. Chen, M. Liu, and H. Deng, 2024: Separation and spatial variations of typhoon and non-typhoon rainfall at different timescales in typical region of southeast China. *Int. J. Climatol.* **44**(13), 4611–4628.

Watanabe, S. I., H. Kawase, Y. Imada, and Y. Hirockawa, 2024: The Impact of anthropogenic global warming and oceanic forcing on the frequency of quasi-stationary band-shaped precipitation systems, "Senjo-Kousuitai", during the rainy season of 2023. *SOLA*, **20A**, 10–18.

Wittek, P., S. C. Gao, I. S. Lim, and L. Zhao, 2017: Somoclu: An Efficient Parallel Library for Self-Organizing Maps. *J. Stat. Softw.* **78**(9), 1–21.

Yoshizaki, M., T. Kato, Y. Tanaka, H. Takayama, Y. Shoji, H. Seko, K. Arao, K. Manabe, and members of X-BAIU 98 observation, 2000: Analytical and numerical study of the 26 June 1998 orographic rainband observed in western Kyushu, Japan. *J. Meteor. Soc. Japan*, **78**(6), 835–856.

Zhang, X., H. Wan, F. W. Zwiers, G. C. Hegerl, and S.-K. Min, 2013: Attributing intensification of precipitation extremes to human influence. *Geophys. Res. Lett.,* **40**(19), 5252–5257.

Zhao, N., A. Manda, X. Guo, K. Kikuchi, T. Nasuno, M. Nakano, Y. Zhang, and B. Wang, 2021: A lagrangian view of moisture transport related to the heavy rainfall of July 2020 in Japan: Importance of the moistening over the subtropical regions. *Geophys. Res. Lett.,* **48**(5), e2020GL091441, doi:10.1029/2020GL091441.

List of Figures

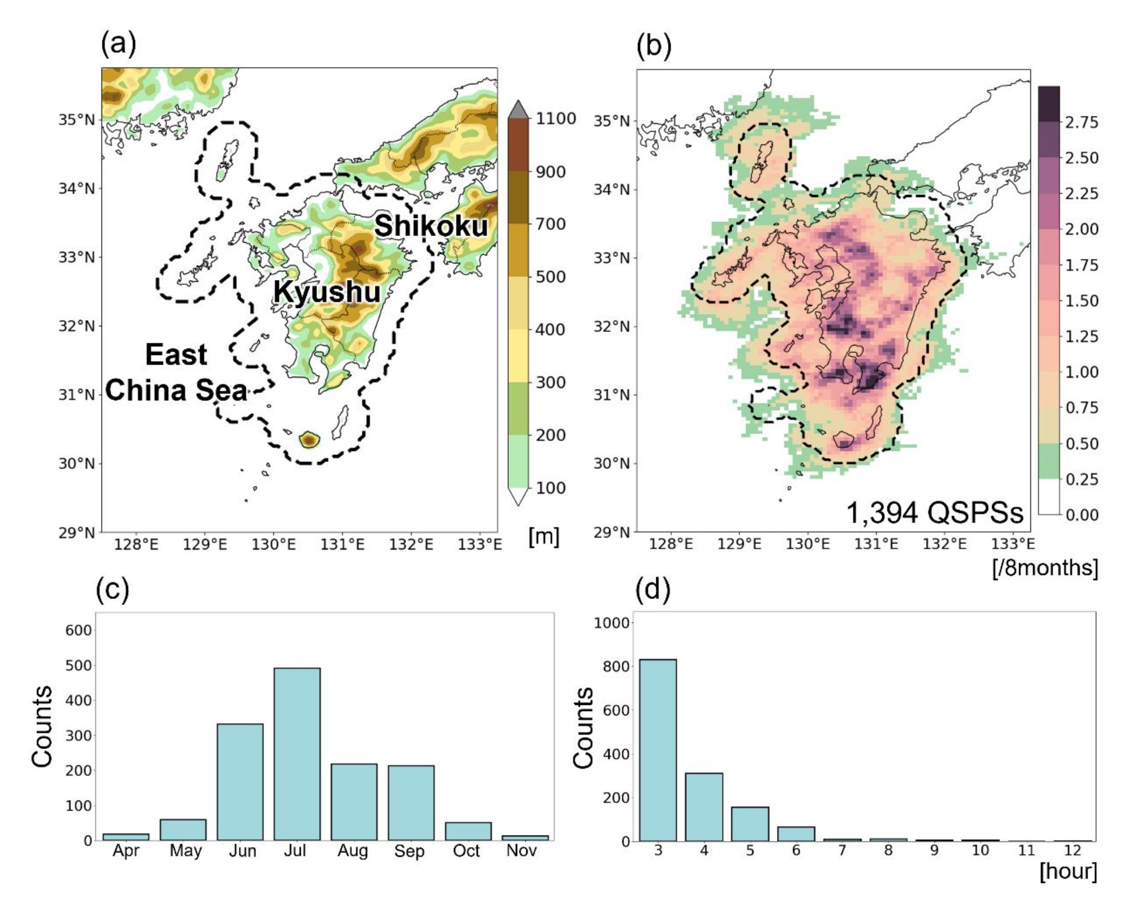

Fig. 1 (a) Topography of Kyushu (shading; m). (b) Distribution of the frequency of QSPSs during April–November, 2006–2023 (shading; /8 months). Dashed line in (a) and (b) indicate the analysis domain. (c) and (d) Occurrence number of QSPSs with respect to month and lifespan, respectively.

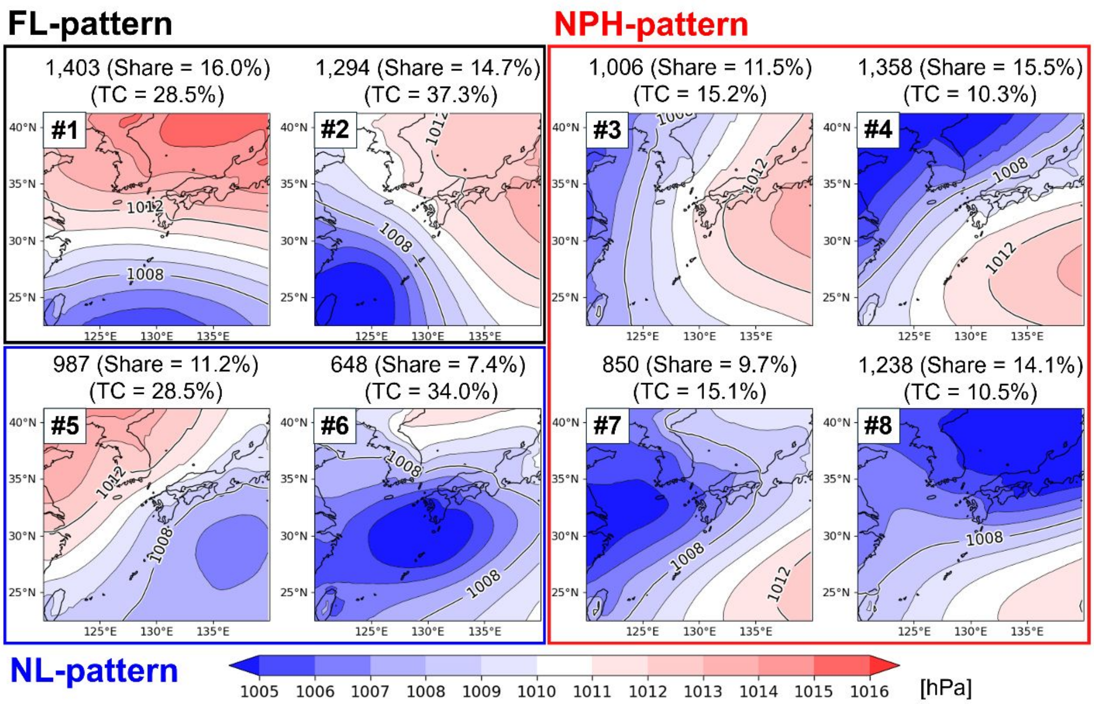

Fig. 2 Composite of SLP (color; hPa) for snapshots classified into each typical SLP pattern during June–September, 2006–2023. The value above each panel indicates the number of SLP snapshots classified and its share. “TC” indicates the percentage of snapshots having tropical cyclone center(s) within the domain. Black, blue, and red frames indicate the FL-pattern (#1 and #2), the NL-pattern (#5 and #6), and the NPH-pattern (#3, #4, #7, and #8), respectively.

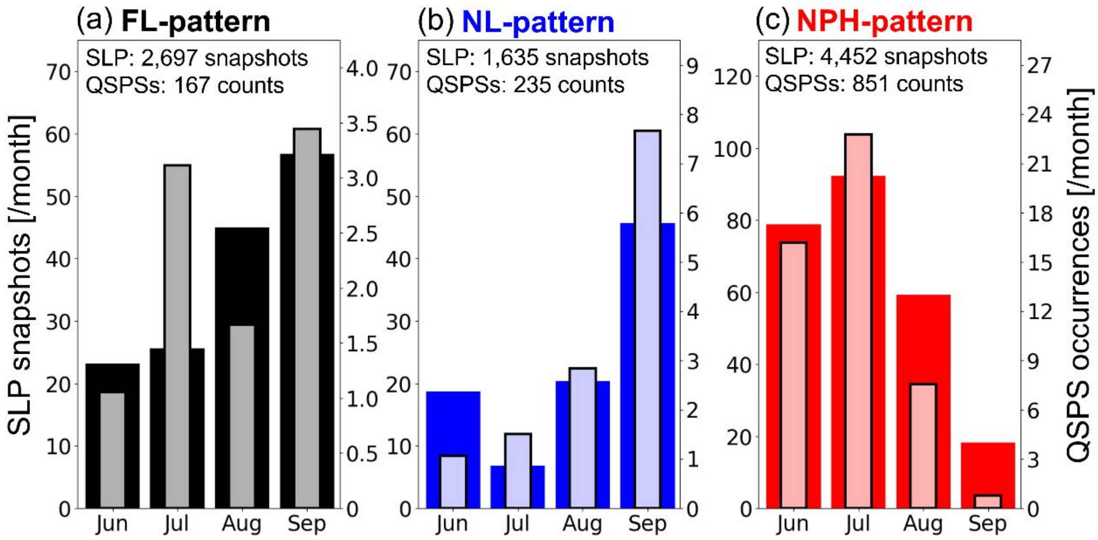

Fig. 3 Monthly variation in classified SLP snapshots (wide bars; left axis) and the number of QSPS occurrences (narrow bars; right axis) during June–September, 2006–2023. Note that the total snapshot number is 30 or 31 days multiplied by 4 snapshots per day (i.e., 120 or 124). (a) the FL-pattern, (b) the NL-pattern, and (c) the NPH-pattern. Total numbers of the SLP snapshots and QSPS occurrences are displayed in each panel.

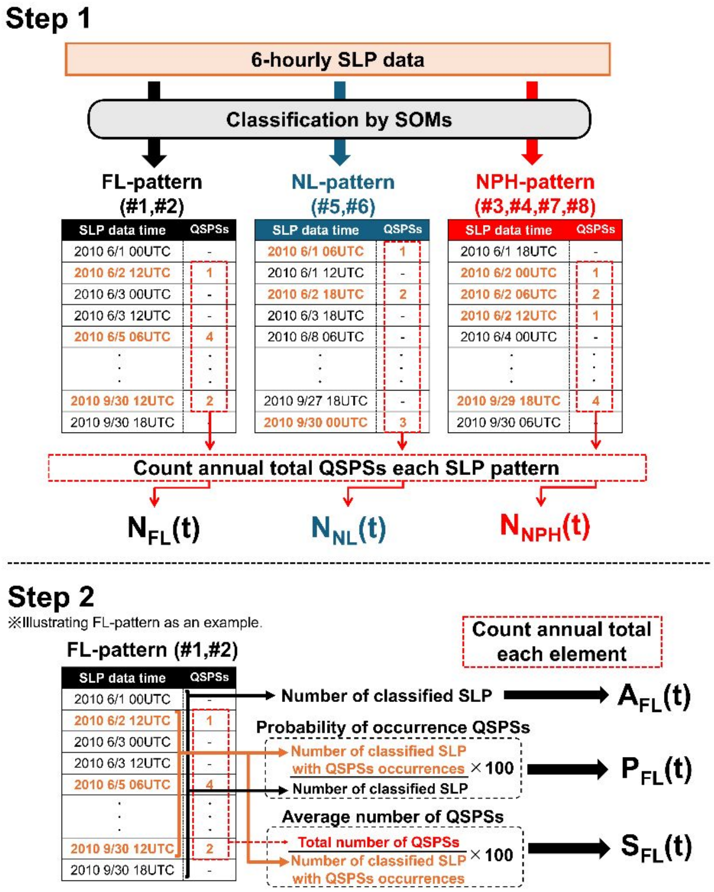

Fig. 4 Schematic of the adopted decomposition method. Step 1 classifies 6-hourly SLP patterns (FL, NL, and NPH) and counts the occurrence number of QSPSs in each SLP pattern for each year (N(t)). Step 2 obtains the interannual variation in the number of QSPSs in the classified SLP pattern (A(t)). The terms P(t) and S(t) represent the proportion of QSPS occurrences per 6-hourly SLP snapshots and the simultaneous QSPS occurrences, respectively. This figure uses the year 2010 as an example.

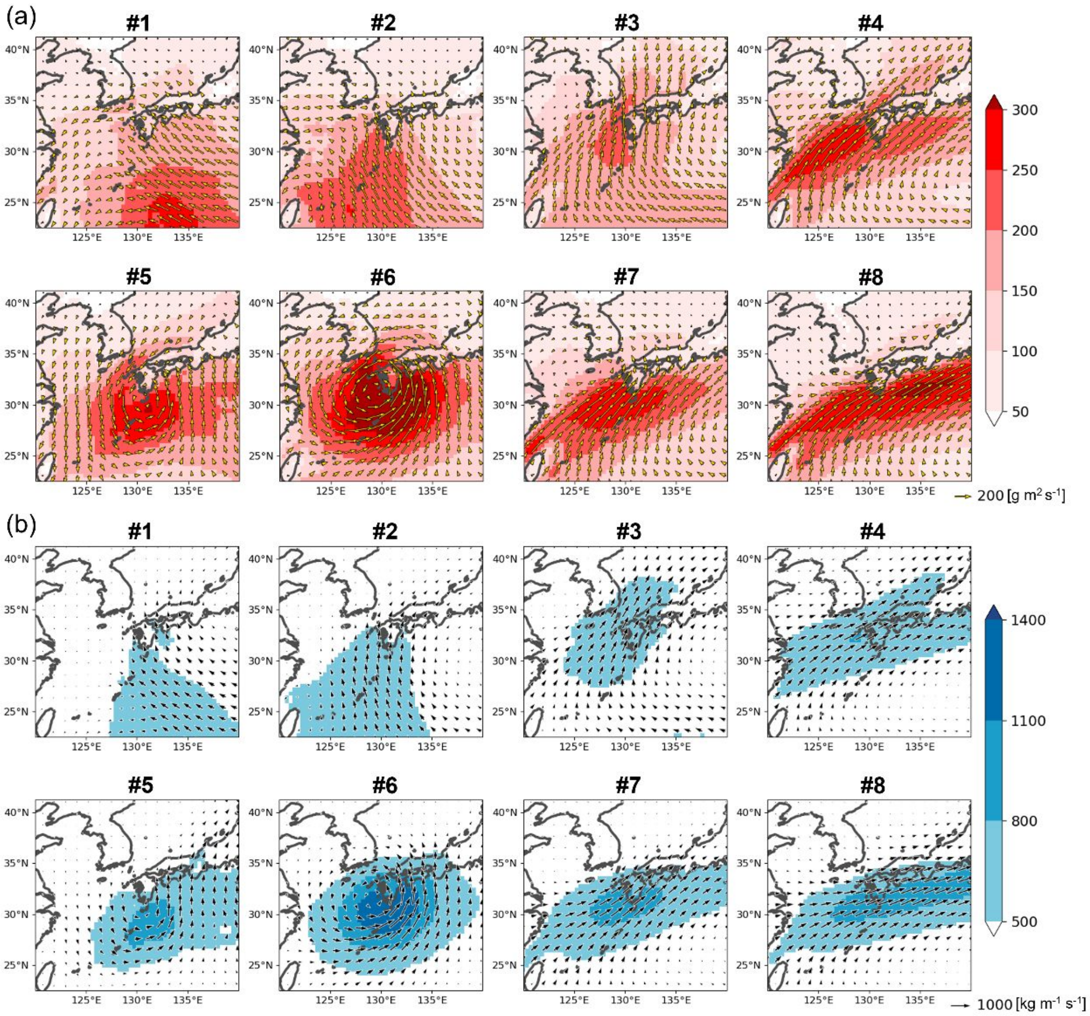

Fig. 5 (a) Composite of the water vapor flux at 500-m heights (vector; g m^{-2} s^{-1}) and its magnitude (shading) and (b) composite of the vertically integrated water vapor transport (vector; kg m^{-1} s^{-1}) and its magnitude (shading) when QSPS occurred in each SLP pattern during June–September, 2006–2023.

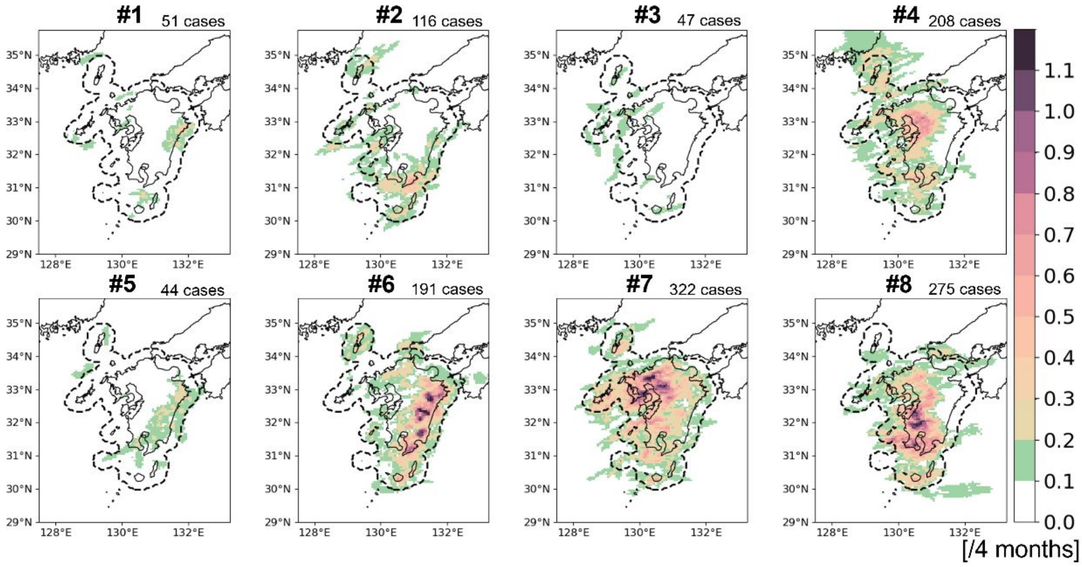

Fig. 6 Distribution of the occurrence number of QSPSs during June–September, 2006–2023 (shading; /4 months) for each SLP pattern. Dashed line indicates the analysis domain.

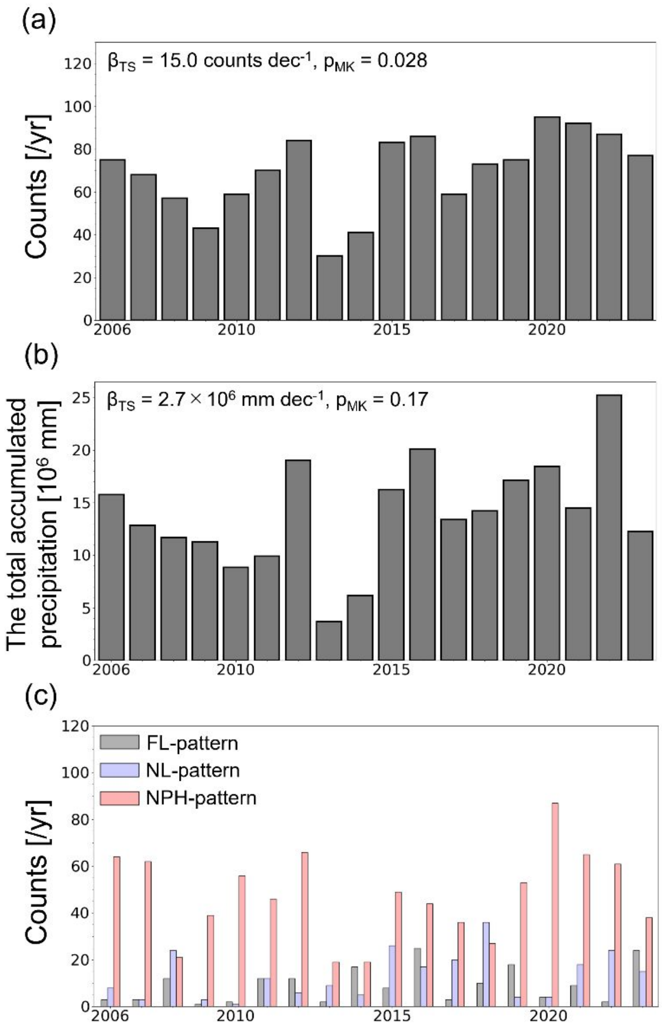

Fig. 7 (a) Interannual variation in the occurrence number of QSPSs. (b) Interannual variation in the total accumulated precipitation of QSPSs. (c) Same as (a), but in each SLP pattern (gray: FL-pattern, blue: NL-pattern, red: NPH-pattern). Statistics, including the p-value from Mann-Kendall trend tests (p_{MK}) and Theil-Sen's slope (β_{TS}; decade^{-1}), are presented in (a) and (b).

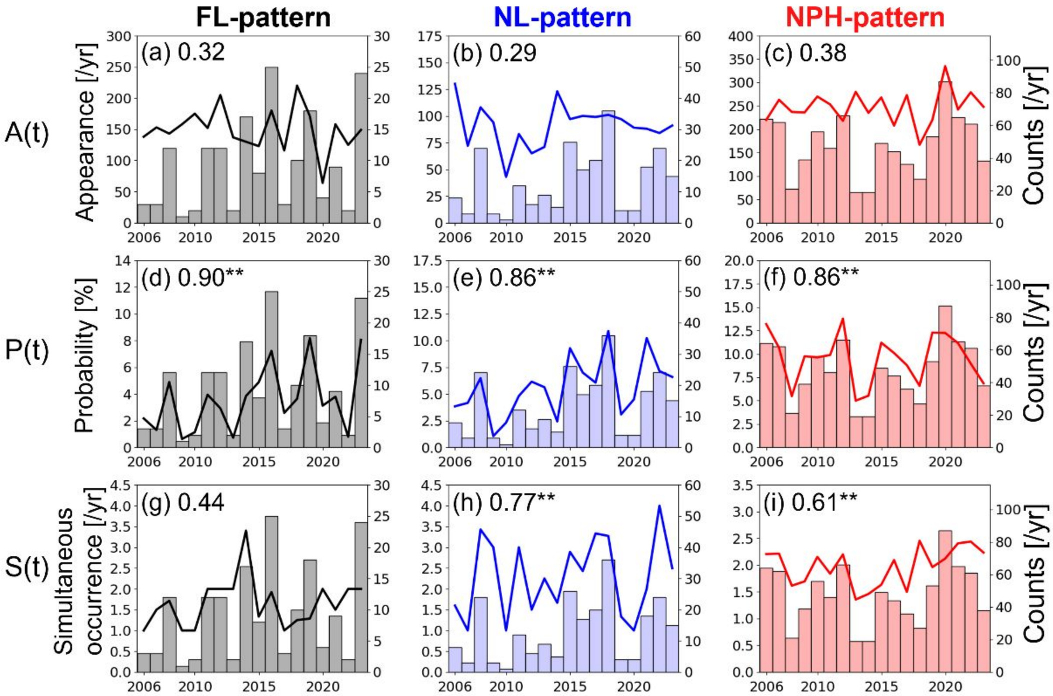

Fig. 8 Interannual variation in the occurrence number of QSPSs in each SLP pattern (bars and right axis, black: FL-pattern, blue: NL-pattern, red: NPH-pattern) and their decomposition parts based on Eq. (2) (lines and left axis): (a)–(c) A(t), (d)–(f) P(t), and (g)–(i) S(t). The value in the upper-left corner of each panel indicates the correlation coefficient. Double asterisks indicate the statistically significant correlation at the 99% confidence level.

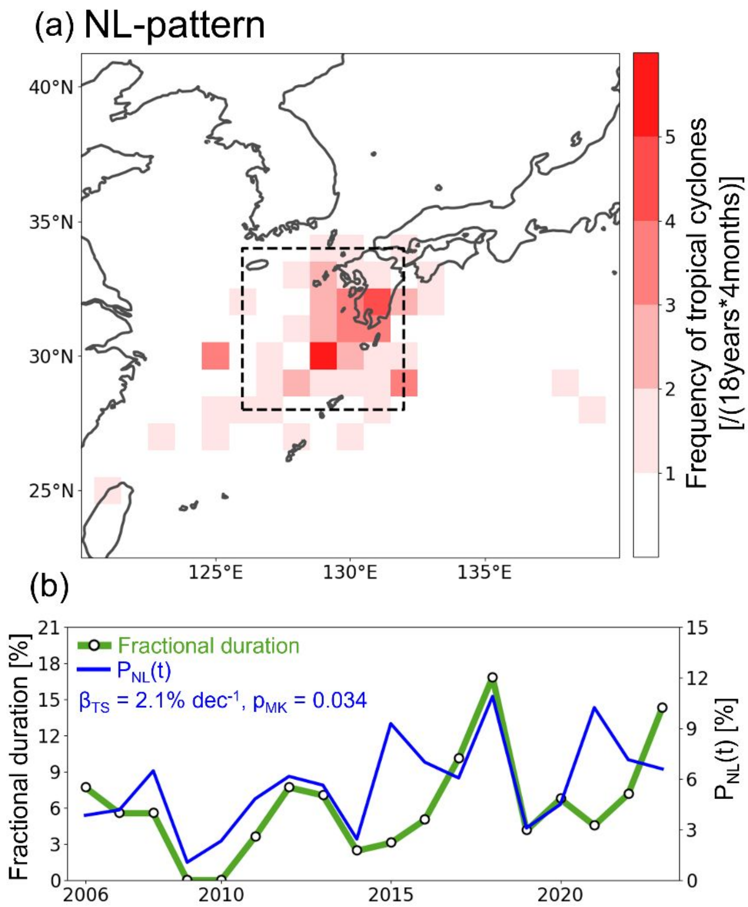

Fig. 9 (a) The number of tropical cyclone centers when QSPSs occurred (color; /(18 years*4 months)) in the NL-pattern. (b) Interannual variation of P(t) (blue line; right axis) and the fractional duration of tropical cyclone presence (green line; left axis) in the NL-pattern. The dashed rectangle in (a) denotes the area (28°–34°N, 126°–132°E) to calculate the fractional duration. Statistics, including the p-value from Mann-Kendall trend tests (p_{MK}) and Theil-Sen's slope (β_{TS}; decade^{-1}), are presented in (b).

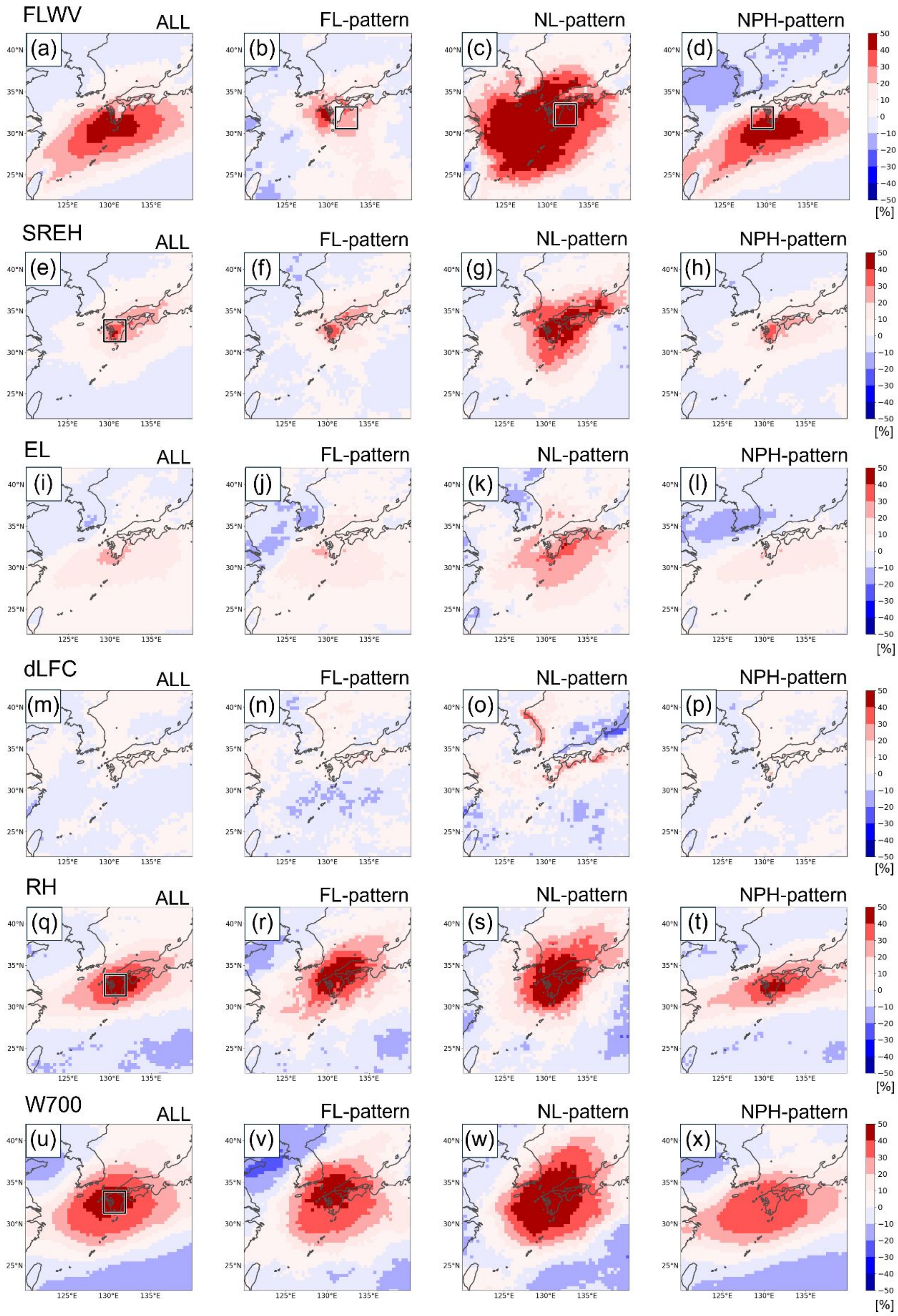
FLWV
ALL
FL-pattern
NL-pattern
NPH-pattern
(a)
(b)
(c)
(d)
SREH
(e)
(f)
(g)
(h)
EL
(i)
(j)
(k)
(l)
dLFC
(m)
(n)
(o)
(p)
RH
(q)
(r)
(s)
(t)
W700
(u)
(v)
(w)
(x)
[%]

Fig. 10 Difference in the fractional duration (%) that satisfies the threshold for each index, comparing the snapshots of with and without QSPS occurrences. (a–d) FLWV, (e–h) SREH, (i–l) EL, (m–p) dLFC, (q–t) RH, and (u–x) W700. From left to right, all SLP patterns, the FL-pattern, the NL-pattern, and the NPH-pattern. Rectangles indicate domains for studying the interannual variation in Fig. 11.

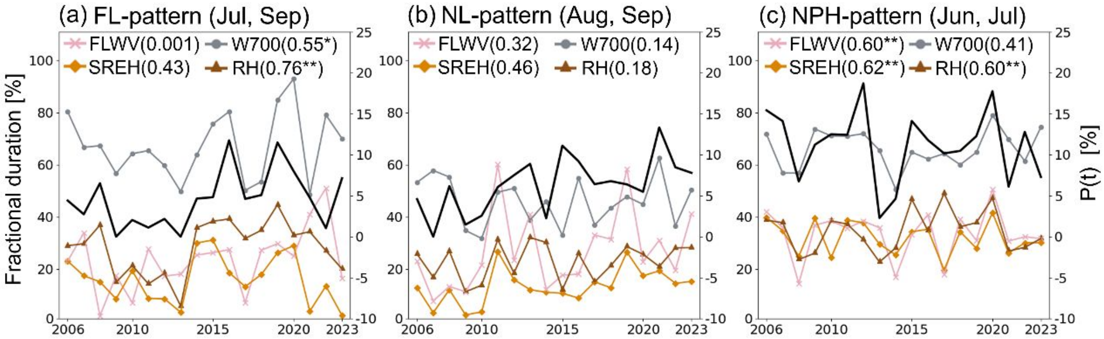

Fig. 11 Interannual variations of P(t) and fractional duration that satisfies the threshold for each index for (a) the FL-pattern, (b) the NL-pattern, and (c) the NPH-pattern. The analysis is based on the two months having the most frequent occurrence of QSPSs as indicated in each panel. The analysis domain is indicated in Fig. 10. The same domain was used across all SLP patterns for SREH, RH, and W700. The correlation coefficient between P(t) and each index is shown, where single and double asterisks denote statistically significant correlation at the 95% and 99% confidence level, respectively.